JOURNAL OF GEOPHYSICAL RESEARCH, VOL. 104, NO. D20, PAGES 24,527–24,545, OCTOBER 27, 1999

Alternative methods for specification of observed forcing in single-column models and cloud system models

David A. Randall and Douglas G. Cripe

Department of Atmospheric Science, Colorado State University, Fort Collins

Abstract. We discuss alternative methods for prescribing advective tendencies in single-column models (SCMs) and cloud system models. These include "revealed forcing," in which the total advective tendency is prescribed from observations; "horizontal advective forcing," in which the horizontal advective tendencies are prescribed, together with the observed vertical motion which is combined with the predicted sounding to determine the tendencies due to vertical advection; and "relaxation forcing," in which the horizontal advective tendencies are computed by relaxing the sounding toward the observed upstream sounding, with a relaxation timescale determined by the time required for the wind to carry parcels across the grid column. When relaxation forcing is used, the horizontal advective tendencies can be diagnosed from the model output and compared with the corresponding observed tendencies. We present SCM results to illustrate these three forcing methods, based on data from several field experiments in both the tropics and the midlatitudes. Each method is shown to have its strengths and weaknesses. Overall, the results presented here do not show unambiguous differences between revealed forcing and horizontal advective forcing. The two methods appear to be generally comparable. Revealed forcing may therefore be preferred for its simplicity. Relaxation forcing guarantees realistic soundings of the state variables but can produce large errors in parameterized processes which are driven by rates (e.g., fluxes) rather than states. In particular, relaxation forcing gives large errors in the precipitation rate in this model. We demonstrate that relaxation forcing leads to unrealistically high (low) precipitation in versions of the model which tend to produce unrealistically dry (humid) soundings. The observed horizontal advective tendencies in the tropics are so weak, especially for temperature, that small absolute errors in the diabatic tendencies diagnosed with relaxation forcing can lead to large relative errors in the diagnosed horizontal advective tendencies.

1. Introduction

Betts and Miller [1986] pioneered the use of single-column modeling as a tool for testing parameterizations developed for use in large-scale models. A single-column model (SCM) is essentially a single grid column of a global model, considered in isolation from the rest of the model. Observations are used to specify what is going on in "neighboring columns," and observations may or may not also be used to specify tendencies due to some parameterized processes, other than those being tested. An SCM is run prognostically; that is, the results obtained for one observation time are used to predict new values of the prognostic variables, which are then provided as input for the next observation time. High-resolution cloud system models (CSMs) can be driven with the same input data [e.g., *Krueger*, 1988]. (We prefer the term "cloud system model" to the more commonly used terms "cumulus ensemble model," "cloud ensemble model," and "cloud-resolving model." An essential aspect of cloud system models is that they have domain sizes much larger than those of individual clouds and that they are used to perform integrations spanning simulated time intervals much longer than the lifetimes of individual cloud elements. The term "cloud-resolving model" is not sufficiently descriptive because it could refer to a model used with a relatively small domain size to simulate the life history of a single cumulus cloud.) This use of SCMs and CSMs to test parameterizations for large-scale atmospheric models has been adopted as a key strategy of the GEWEX Cloud Systems Study (GCSS) [*Browning*, 1993].

Paper number 1999JD900765.
0148-0227/99/1999JD900765$09.00

Randall et al. [1996a] summarized a strategy for testing parameterizations in SCMs. The SCM is driven with observations; the methods used for doing this are the main subject of this paper and are discussed in detail below. The results produced by the SCM are compared with additional observations of the same meteorological events. If a CSM is driven with the same data, then the results of the CSM can be compared with those of the SCM and also, of course, with observations. When the SCM parameterizations are judged to have performed satisfactorily in tests against observations, they can be transplanted into a three-dimensional atmospheric general circulation model (GCM). As discussed later, it is possible to incorporate an SCM into the framework of a GCM, in which case the SCM parameterizations are available immediately for use in the GCM, with little additional work.

In the research strategy outlined above, an SCM and a CSM are forced with observed, objectively analyzed fields. There are many possible ways to do this. Consider an arbitrary scalar variable q, satisfying a conservation equation in "flux form":

$$\frac{\partial q}{\partial t} = -\left[\nabla \cdot (\mathbf{V}q) + \frac{\partial}{\partial p} (\omega q) \right] + P. \qquad (1)$$

Here P represents the "physics" that affects q. (We are using pressure coordinates in this discussion, for simplicity. Essentially the same points could be made using other vertical coordinate systems.) The continuity equation corresponding to (1) is

$$\nabla \cdot \mathbf{V} + \frac{\partial \omega}{\partial p} = 0. \tag{2}$$

By using (2) in (1), we can rewrite our conservation equation in "advective form":

$$\frac{\partial q}{\partial t} = -\left(\mathbf{V} \cdot \nabla q + \omega \frac{\partial q}{\partial p} \right) + P. \tag{3}$$

Neither an SCM nor a CSM can predict the horizontally domain-averaged divergence $\nabla \cdot \mathbf{V}$, so if (2) is to be used to obtain the vertical velocity, then $\nabla \cdot \mathbf{V}$ must be prescribed from observations. Similarly, neither an SCM nor a CSM can determine the horizontally domain-averaged horizontal advective tendency, $-\nabla \cdot (\mathbf{V}q)$ or $-\mathbf{V} \cdot \nabla q$, so it is necessary to prescribe some information about the horizontal advection of q. In addition, it can sometimes be useful to prescribe some part of the parameterized physical tendency represented by P, although, of course, the whole point of the calculations with the SCM is to test some of the parameterized processes of the model against observations, so at most only part of P is prescribed. Concrete examples will be given later.

The observed temperatures, water vapor mixing ratios, and winds needed to drive an SCM or CSM are objectively analyzed [e.g., *Barnes*, 1964]. It is also necessary to evaluate the horizontal advection term of (3), averaged over the region of interest. The objectively analyzed thermodynamic soundings, wind profiles, and large-scale divergence are averaged over the same region. The divergence is typically corrected to ensure mass conservation consistent with the observed surface pressure tendency; additional corrections can be made to ensure conservation of dry air, moisture, energy, etc. [e.g., *O'Brien*, 1970; *Zhang and Lin*, 1997]. The data are used to specify the horizontal advection term of (3), as well as the vertical velocity ω which is used in the vertical advection term.

Besides pure objective analysis, it is also possible to use analyses generated through data assimilation. The advantages and disadvantages of such a procedure are often debated, but that subject falls outside the scope of the present paper.

Some investigators have experimented with an artificial "relaxation" term added to the right-hand side of (3); that is,

$$\frac{\partial q}{\partial t} = -\left(\mathbf{V} \cdot \nabla q + \omega \frac{\partial q}{\partial p} \right) + P + \frac{(q_{\text{obs}} - q)}{\tau}, \tag{4}$$

where q_{obs} is the observed value of q, and τ is a specified "relaxation timescale," which is specified to be of the order of a day to perhaps half a day. The effect of the relaxation term is to prevent the predicted value of q from drifting very far away from the observed value q_{obs}. A problem with the relaxation term is that it does not represent any real physical process.

The purpose of this paper is systematically to examine (boldly to go) and compare various ways in which the large-scale advective tendencies can be prescribed as forcing terms in the prognostic equation for q. Section 2 surveys several such forcing methods and discusses their relative advantages and disadvantages from an "a priori" perspective. Section 3 describes the several data sets used in the evaluations. Section 4 describes the particular SCM which is used, in this paper, to evaluate the forcing methods. Section 5 presents results obtained with the various methods, as applied to the observed cases. Section 6 gives a summary and conclusions.

2. Methods for Prescribing Advective Tendencies

2.1. Revealed Forcing

One approach to specifying the large-scale advective forcing is simply to compute $-(\mathbf{V} \cdot \nabla q + \omega\, \partial q/\partial p)$ directly from the analyzed observations [e.g., *Redelsberger et al.*, 1998; *Bechtold et al.*, 1998], and then prescribe these values in the SCM:

$$\frac{\partial q}{\partial t} = -\left(\mathbf{V} \cdot \nabla q + \omega \frac{\partial q}{\partial p} \right)_{\text{obs}} + P. \tag{5}$$

We refer to this as "revealed (because it is given unto you) forcing." With this simple approach, errors in the predicted vertical distribution of q have no effect on the advective tendency of q. Revealed forcing is very simple, but it fails to take into account how simulated changes in the sounding would affect the tendencies due to vertical advection. For example, if in the course of an integration a segment of the simulated sounding becomes dry adiabatic, temperature changes due to dry adiabatic vertical motions are impossible, but with revealed forcing, the tendency of the temperature due to vertical motion is precomputed from the observations and so cannot respond to such changes in the sounding.

2.2. Horizontal Advective Forcing

A simple modification of revealed forcing, which we call horizontal advective forcing, consists of prescribing $-\mathbf{V} \cdot \nabla q$ and ω from the observations, and using the predicted profile of q, together with the prescribed ω, to evaluate $-\omega(\partial q/\partial p)$ as the model runs:

$$\frac{\partial q}{\partial t} = -(\mathbf{V} \cdot \nabla q)_{\text{obs}} - \omega_{\text{obs}} \frac{\partial q}{\partial p} + P. \tag{6}$$

Horizontal advective forcing allows the tendency of q, due to vertical advection, to depend on the predicted profile of q, as it does in nature and as it would in a full three-dimensional model; this dependency is missing with revealed forcing.

A very similar approach can be followed using the flux form rather than the advective form. Splitting the horizontal advection term of (1) into two pieces gives

$$\frac{\partial q}{\partial t} = -\left[\mathbf{V} \cdot \nabla q + q(\nabla \cdot \mathbf{V}) + \frac{\partial}{\partial p} (\omega q) \right] + P. \tag{7}$$

Observations can be used to prescribe $\mathbf{V} \cdot \nabla q$ and $\nabla \cdot \mathbf{V}$. By integrating the continuity equation (equation (2)), we can obtain $\omega_{\text{obs}}(p)$ from $(\nabla \cdot \mathbf{V})_{\text{obs}}$; that is,

$$\omega_{\text{obs}}(p) = -\int_0^p (\nabla \cdot \mathbf{V})_{\text{obs}}\, dp. \tag{8}$$

Then (7) can be written as

$$\frac{\partial q}{\partial t} = -\left[(\mathbf{V} \cdot \nabla q)_{\text{obs}} + q(\nabla \cdot \mathbf{V})_{\text{obs}} + \frac{\partial}{\partial p} (\omega_{\text{obs}} q) \right] + P. \tag{9}$$

It is important that the finite-difference operator used to approximate $(\partial/\partial p)(\omega_{\text{obs}} q)$ in (9) reduce to the finite-difference

operator for $(\partial \omega_{\text{obs}}/\partial p)$ in (8), when q is replaced by unity. When this is the case, vertical advection cannot generate variations of q when none are present initially.

2.3. Relaxation Forcing

Consider (1), i.e., the flux form of the prognostic equation for q. Using the Gauss theorem, we can rewrite the horizontal flux divergence term of (1) as

$$\nabla \cdot (\mathbf{V}q) = \frac{1}{A} \oint (V_n q)\, dl, \tag{10}$$

where the line integral is taken around the boundary of the region, A is the area of the region, and V_n is the outward normal component of $\mathbf{V}$. We can divide this line integral into two parts: the integral over the portion of the boundary where the wind is blowing into the region and the integral over the portion of the boundary where the wind is blowing out of the region. Then (10) becomes

$$\nabla \cdot (\mathbf{V}q) = \frac{1}{A} [-(V_{\text{in}} \Delta l_{\text{in}} q_{\text{in}}) + (V_{\text{out}} \Delta l_{\text{out}} q_{\text{out}})], \tag{11}$$

where the first term represents the inflow (hence the minus sign) and the second represents the outflow. Note that we have defined V_{in} and V_{out} in such a way that

$$V_{\text{in}} \geq 0 \quad \text{and} \quad V_{\text{out}} \geq 0 \tag{12}$$

are guaranteed.

Next, we modify (11) by adding and subtracting terms involving q, where q is interpreted as the area-averaged value of q for the cell

$$\nabla \cdot (\mathbf{V}q) = \frac{1}{A} \{-[V_{\text{in}} \Delta l_{\text{in}} (q_{\text{in}} - q)] + [V_{\text{out}} \Delta l_{\text{out}} (q_{\text{out}} - q)]\}$$

$$+ \frac{q}{A} [-(V_{\text{in}} \Delta l_{\text{in}}) + (V_{\text{out}} \Delta l_{\text{out}})]. \tag{13}$$

We recognize the quantity on the second line of the right-hand side of (13) as $q \nabla \cdot \mathbf{V}$, so (13) is equivalent to

$$\nabla \cdot (\mathbf{V}q) = \frac{1}{A} \{-[V_{\text{in}} \Delta l_{\text{in}} (q_{\text{in}} - q)] + [V_{\text{out}} \Delta l_{\text{out}} (q_{\text{out}} - q)]\}$$

$$+ q \nabla \cdot \mathbf{V}, \tag{14}$$

or

$$\mathbf{V} \cdot \nabla q = \frac{1}{A} \{-[V_{\text{in}} \Delta l_{\text{in}} (q_{\text{in}} - q)] + [V_{\text{out}} \Delta l_{\text{out}} (q_{\text{out}} - q)]\}. \tag{15}$$

Equation (15) is essentially a finite-difference scheme, which can be used to diagnose $\mathbf{V} \cdot \nabla q$; each of the quantities on the right-hand side of (15) can be inferred from a sufficiently detailed set of data.

Now suppose that

$$q - q_{\text{out}} = f(q_{\text{in}} - q), \tag{16}$$

which is equivalent to

$$q = \frac{q_{\text{out}} + f q_{\text{in}}}{1 + f}. \tag{17}$$

Equation (16) is nothing more than the definition of f. The data can be used to compute f for a given observation time, and the data together with model results can be used to compute f for a given simulation time. For

$$f \geq 0, \tag{18}$$

q is bounded by q_{out} and q_{in}, or in other words, q changes monotonically across the grid cell. For $f = 1$, (16) reduces to $q - q_{\text{out}} = q_{\text{in}} - q$, which simply means that q lies half way between q_{in} and q_{out}; this should be approximately true in most cases, so we expect that f will often be close to 1. When $f < 0$, the grid cell contains a local maximum or minimum of q.

With the use of (16) we can rewrite (15) as

$$-\mathbf{V} \cdot \nabla q = \frac{q_{\text{in}} - q}{\tau_{\text{adv}}}, \tag{19}$$

where we define

$$\frac{1}{\tau_{\text{adv}}} \equiv \frac{(V_{\text{in}} \Delta l_{\text{in}}) + f(V_{\text{out}} \Delta l_{\text{out}})}{A}. \tag{20}$$

So long as (18) is satisfied, we are guaranteed that

$$\tau_{\text{adv}} \geq 0. \tag{21}$$

This essentially follows from (12). Note that (21) can be satisfied even for $f < 0$. Equations (19) and (20) are analogous to an "upstream" advection scheme for a numerical model.

To get a feeling for (20), consider the following examples, for which we assume that $V_{\text{in}} = V_{\text{out}} = V$ and $\Delta l_{\text{in}} = \Delta l_{\text{out}} = \Delta l$, so (20) reduces to $(1/\tau_{\text{adv}}) \equiv [V \Delta l(1 + f)]/A$. First, consider a square cell of side d. If inflow and outflow both span two cell walls, then we get $(1/\tau_{\text{adv}}) \equiv [2V(1 + f)]/\sqrt{A}$. As a second example, consider a circular grid cell, of radius r. In this case, $A = \pi r^2$ and $\Delta l = \pi r$, so we get $(1/\tau_{\text{adv}}) = [\sqrt{\pi} V(1 + f)]/\sqrt{A}$. Since $\sqrt{\pi} \cong 2$, these two examples have given practically the same result.

Finally, we substitute (19) in (13) to obtain

$$\frac{\partial q}{\partial t} = \frac{q_{\text{in}} - q}{\tau_{\text{adv}}} - \omega \frac{\partial q}{\partial p} + P. \tag{22}$$

The meaning of (19) and (22) is that horizontal advection acts like a relaxation of q toward q_{in}, with relaxation timescale τ_{adv}. We can use (22) to predict q, utilizing the predicted value of q on the right-hand side. This means that the horizontal advection term of (22) is determined partly through the observed values of q_{in} and τ_{adv} and partly through the simulated value of q. Obviously the relaxation term of (22) drives q toward q_{in}, so if τ_{adv} is short enough (i.e., if the advecting wind is strong enough) then q cannot be very different from q_{in}.

When we directly insert the observed value of $-(\mathbf{V} \cdot \nabla q)_{\text{obs}}$ into (9), we provide information about the gradient of q but not about the actual value of q. The SCM is started from the observed value of q, but after some time, errors in the prescribed horizontal advective tendency and/or errors in the SCM physics can drive the simulated sounding away from the evolving observed sounding; the model "gets lost." This can happen because of errors in the observed advective tendencies, even if the SCM physics is perfect. Because the inserted data do not contain information about the actual value of q, the model cannot find its way back home, i.e. to return to a sounding that is in agreement with the observations.

Compare (22) with (4). The relaxation term of (4) is added artificially, in addition to the horizontal advection term. The relaxation timescale in (4) is arbitrarily specified. The relaxation in (4) is toward q_{obs}, the observed value of q in the

region. The relaxation term of (4) cannot be compared with observations because it does not represent a real physical process; one could say, however, that the observed value of the relaxation term of (4) is zero.

In contrast, the relaxation term of (22) is identically the horizontal advection term. The relaxation timescale τ_{adv} can be computed directly from the wind data and does not have to be specified arbitrarily. The relaxation in (22) is toward q_{in}, the observed property of the air entering the region. The relaxation term of (22) can be compared with the objectively analyzed value of $-\mathbf{V} \cdot \nabla q$, which varies with time and height.

Before we can actually use (22), it is necessary to diagnose q_{in} and τ_{adv} from the objective analysis scheme. We make the following simplifying assumptions: $f = 1$; $V_{in} = V_{out} \equiv V$, where V is the average wind speed in the region; and $\Delta l_{in}/A = \Delta l_{out}/A = 1/d$, where d is a length scale that is closely related to the distance across the region (depending on wind direction). Then (20) reduces to

$$\frac{1}{\tau_{adv}} = \frac{2V}{d}, \tag{23}$$

and (19) yields

$$q_{in} = q - \tau_{adv}\mathbf{V} \cdot \nabla q. \tag{24}$$

All of the quantities on the right-hand sides of (23) and (24) are observable. With this approach, we can diagnose values of τ_{adv} and q_{in} directly from the observations. These values can then be used with the SCM and/or the CSM. (Equation (20), which has been used to estimate the relaxation timescale, implies nondivergent flow in the sense that using (20) and setting $q \equiv 1$ in (11) yields the statement that the horizontal divergence is equal to zero. If (11) were modified to include the effects of divergence, this change would give a different relaxation timescale but only slightly different. Moreover, (20) is not used to determine the horizontal divergence or the vertical velocity; as explained above, these quantities are obtained by an approach that makes no use of (20) or (11) and makes no use of the relaxation timescale.)

Using (24), we can write the observed advective tendency as

$$-(\mathbf{V} \cdot \nabla q)_{obs} = (q_{in} - q_{obs})/\tau_{adv}. \tag{25}$$

Suppose that we predict q using an SCM; let the predicted value be denoted by q_{model}. We can then diagnose the advective tendency, as implied by the model results, as

$$-(\mathbf{V} \cdot \nabla q)_{model} = (q_{in} - q_{model})/\tau_{adv}. \tag{26}$$

Comparing (25) and (26), we see that

$$\frac{(q_{in} - q_{model})}{\tau_{adv}} = \frac{(q_{in} - q_{obs})}{\tau_{adv}} + \frac{(q_{obs} - q_{model})}{\tau_{adv}}, \tag{27}$$

or

$$-(\mathbf{V} \cdot \nabla q)_{model} = -(\mathbf{V} \cdot \nabla q)_{obs} + \frac{q_{obs} - q_{model}}{\tau_{adv}}. \tag{28}$$

Use of advective relaxation means integration of

$$\frac{\partial q_{model}}{\partial t} = -(\mathbf{V} \cdot \nabla q)_{model} - \omega_{obs}\frac{\partial q_{model}}{\partial p} + P. \tag{29}$$

This is just (22) again but with subscripts added for clarity of exposition. Using (28) in (29), we see that advective relaxation is equivalent to use of

$$\frac{\partial q_{model}}{\partial t} = -(\mathbf{V} \cdot \nabla q)_{obs} + \frac{q_{obs} - q_{model}}{\tau_{adv}} - \omega_{obs}\frac{\partial q_{model}}{\partial p} + P. \tag{30}$$

Equation (30) was discussed by *Ghan et al.* [1999a]. Compare (30) with (4) to see that advective relaxation is equivalent to the use of (4), provided that the relaxation timescale in (4) is prescribed, from the observations, as τ_{adv}. Note, however, that if the model is giving the right answer, i.e., if $q_{model} = q_{obs}$, then the relaxation term of (30) will vanish. This is consistent with our earlier assertion that this term does not represent a real physical process.

2.4. Discussion

In this paper we present results obtained with all three of the methods outlined above. The emphasis is on documenting and discussing the advantages and disadvantages of each of the three methods. Before going on to examine the results, we suggest some plausible hypotheses about what we will find.

1. Relaxation forcing will give the best overall results, not only for the temperature and moisture soundings but also for the parameterized physical processes, which have a better chance to work as intended when presented with realistic soundings.
2. Horizontal advective forcing will give the worst overall results, because errors in the simulated soundings will give rise to errors in the tendencies due to vertical advection, which will lead to further errors in the soundings, etc.
3. Revealed forcing will give better results than horizontal advective forcing, because the advective tendencies are prescribed from the data and therefore are not corrupted by errors produced as the model runs.

Results presented later show that these hypotheses are partly right and partly wrong.

3. Data Used

Three types of data are needed for use with SCMs and CSMs: initial conditions for the prognostic variables; boundary conditions, including forcing functions such as the large-scale divergence; and data for evaluation of the model results.

The data used in the present study came from three sources: (1) the Southern Great Plains site of the Atmospheric Radiation Measurements (ARM) Project; (2) the Global Atmospheric Research Program (GARP) Atlantic Tropical Experiment (GATE); and (3) the Tropical Ocean Global Atmosphere Coupled Ocean-Atmosphere Response Experiment (TOGA COARE). A brief description of these data sets follows.

3.1. ARM

ARM's Southern Great Plains (SGP) site in north central Oklahoma and south central Kansas [*Stokes and Schwartz*, 1994] (see Figure 1) furnished data for six of the SCM simulations discussed in the present study.

A variety of instruments collect data at the ARM site on an ongoing basis. In addition, intensive observation periods (IOPs) are conducted quasi-periodically throughout the year, most lasting ~3 weeks. During these IOPs, data are collected with increased frequency, and in particular radiosondes are launched every 3 hours from four positions around the perimeter of the site, as well as from its center. The four launch positions on the periphery of the site coincide with the locations of National Oceanic and Atmospheric Administration wind profilers. Precipitation data were provided by the Oklahoma mesonet and Kansas State University mesonet systems in addition to that reported from Surface Meteorological Observing System (SMOS) automated sensors at various locations

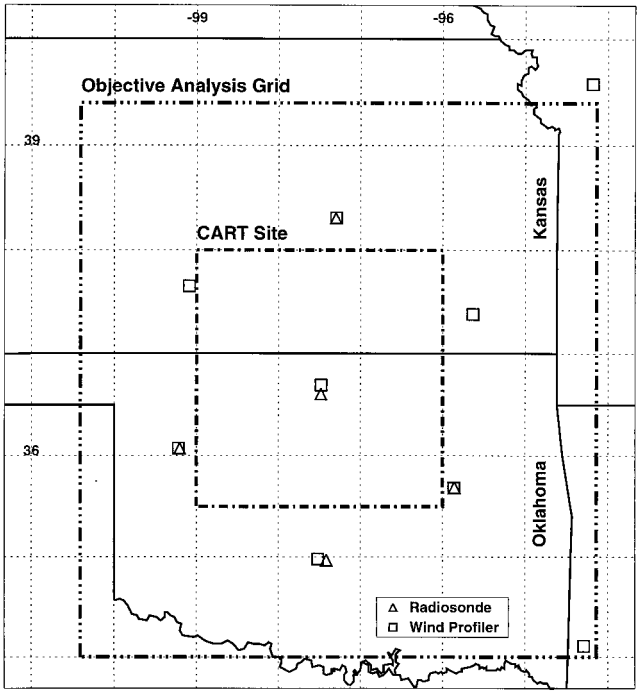

Figure 1. Location of Atmospheric Radiation Measurement (ARM) Southern Great Plains (SGP) radiosonde launch sites (triangles), wind profilers (squares), CART (cloud and radiation test bed) site, and objective analysis grid.

around the SGP CART site. Table 1 summarizes the dates and weather conditions of the IOPs that generated the ARM data sets used in this study.

The data obtained from the radiosondes and wind profilers were subjected to objective analysis [*Leach et al*., 1996, 1997]. This included an initial check for outliers and temporal interpolation to fill in missing data and to replace spurious data. Wind profiler data were interpolated from height to pressure surfaces and combined with the processed radiosonde data. Finally, a *Barnes* [1964] objective analysis scheme was employed with the merged wind profiler and radiosonde data. For further discussion, see *Leach et al*. [1996, 1997]. For the July 1995 IOP only, we used a modified version of the objectively analyzed data, which has been subjected to variational constraints, as discussed by *Zhang and Lin* [1997].

Because the ARM data comes from a land site and because our study focuses on cloud processes in the atmosphere, we prescribed the surface fluxes from the observations. We used the energy balance Bowen ratio (EBBR) fluxes of sensible and latent heat and applied some simple quality control procedures. First, the data stream from each station (total of 10) was examined individually to check for missing data. Whenever an observation was determined to be missing, a flag was inserted into the data stream at that point to fill in the gaps. This step was necessary to synchronize the observations across all the stations. Next obvious outliers were eliminated, then the Bowen ratio associated with each observation time was checked to determine whether it fell within reasonable limits. If not, the data point was flagged as "missing." A further test was conducted to establish whether the instrument sensors were in the correct position at the time of observation. Again, data points that failed this test were flagged as missing. Following these checks, the data from all 10 stations were examined at each observation time and a final average was computed among those stations reporting valid data at that particular time. This average could be composed of data from 1 to 10 stations, depending on the amount of missing data. An example for the July 1995 IOP is shown in Figure 2. The figure shows the surface sensible and latent heat fluxes before and after application of the quality control procedures described above.

3.2. GATE

The GATE data used here are based on *Ooyama*'s [1987] scale-controlled objective analysis of the data obtained by a network of ship observations and radiosonde launches in the eastern Atlantic Intertropical Convergence Zone during Phase III of GATE, as described by *Reed et al*. [1977] and *Thompson et al*. [1979]. Surface precipitation rates were provided by 3-hourly radar observations [*Hudlow and Patterson*, 1979]. Estimates of the surface fluxes were obtained from E. Recker of the University of Washington (personal communication, 1996).

3.3. TOGA COARE

We used the TOGA COARE analyses of *Lin and Johnson* [1996a, b]. All wind and thermodynamic data from the soundings were objectively analyzed using multiquadratic interpolation [*Nuss and Titley*, 1994] onto a $1° \times 1°$ grid over the TOGA COARE Large Scale Array. The 25 data points that fell within the perimeter of the Intensive Flux Array (IFA) were averaged together. These analyses were carried out for all 480 of the 6-hourly observations collected during TOGA COARE. Rainfall rates were computed by subtracting averaged surface evaporation rates from the net surface moisture source as inferred by vertical integration of the analyzed apparent moisture sink [*Yanai et al*., 1973]. Sea surface temperatures and surface fluxes represent the averages of measurements collected at several buoys in the IFA.

3.4. Discussion

The wide variety of data used in this study are summarized in Table 2. The GATE and TOGA COARE data were col-

Table 1. Summary of Dates and Durations of ARM IOPs and Sketch of Weather Conditions Encountered

IOP Dates	Number of Days	Weather Conditions
Oct. 25 to Nov. 13, 1994	20	precipitation fairly cyclic, falling every 3–4 days, with intensity tapering off through the IOP
April 20 to May 7, 1995	18	several days of light rain, with some heavier rain showers near the end of the IOP
July 18 to Aug. 3, 1995	17	frequent moderate showers in first half of IOP, then 5 dry days and then more rain at end of IOP
Sept. 23 to Oct. 20, 1995	28	a few light to moderate rain events during the first weeks, then dry for second 2 weeks of IOP
April 16 to May 5, 1996	20	three main rain events, spaced about every 6 days, with heaviest event in middle of IOP
July 16 to Aug. 4, 1996	20	light showers during the first 6 days, then light to moderate showers every other day for the remainder of the IOP

IOP, intensive observation period; ARM, Atmospheric Radiation Measurement.

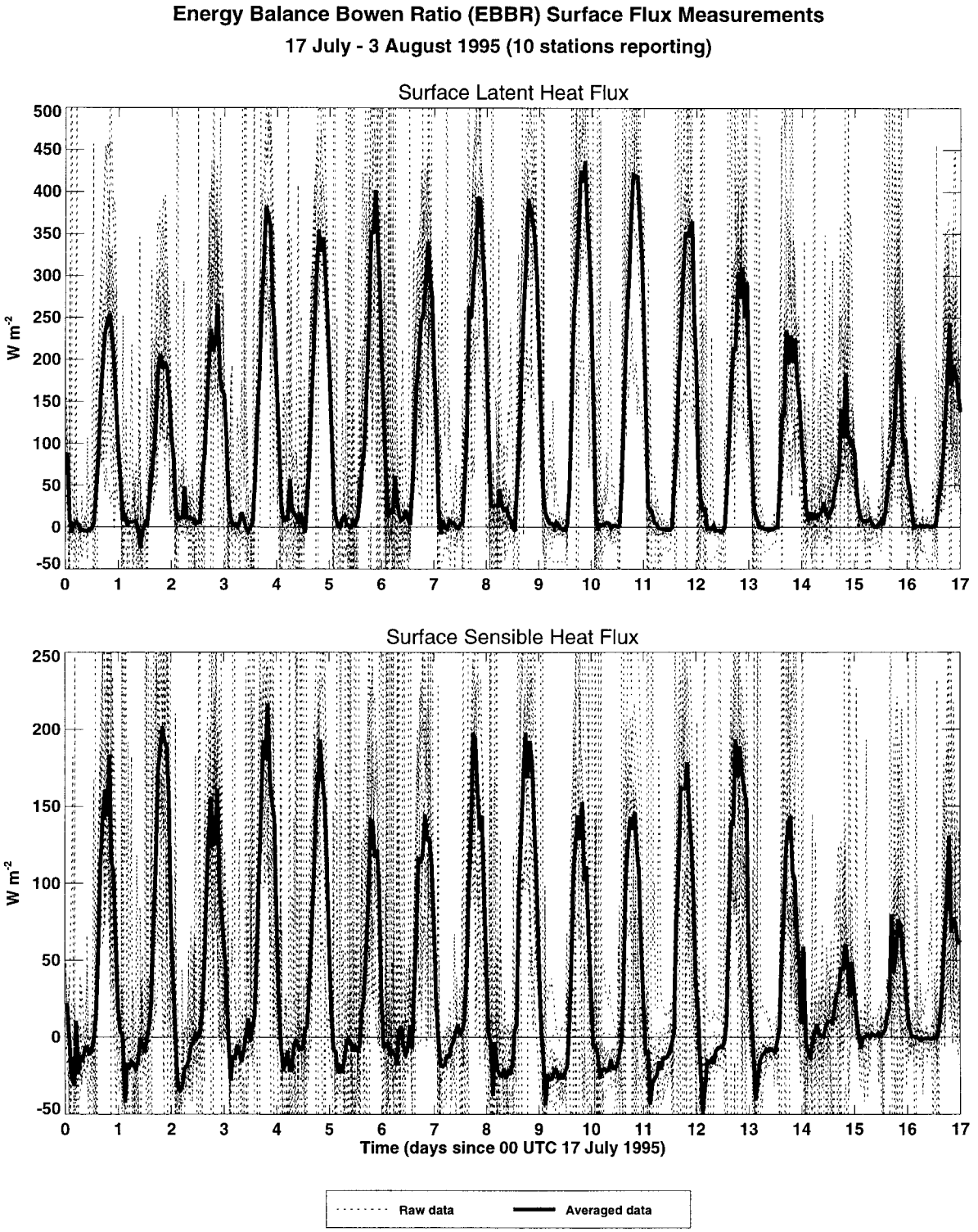

Figure 2. Time series of the surface sensible and latent heat fluxes used for the July 1995 ARM intensive observation periods (IOP). Similar data sets were prepared for the other ARM IOPs and were obtained for GATE and TOGA COARE; these are not plotted here, for brevity.

lected in warm, convectively active regions of the tropical oceans. In contrast, the ARM data are from a midlatitude land site. The ARM data include warm-season, convectively active, and cool-season IOPs. The data used in this study allow us to explore the strengths and weaknesses of the various SCM forcing strategies for both tropical and seasonally varying extratropical conditions. In GATE and TOGA COARE the temporal fluctuations of temperature (especially) and moisture are quite small. In addition, as illustrated in Figure 3, the horizontal advection term of (3) is quite small, especially for the case of temperature. The well-known explanation is that in the tropics, strong pressure gradients are (except in tropical cy-

Table 2. Summary of Data Used in This Study

Data Requirement	ARM	GATE	TOGA COARE
		Initial Conditions	
Temperature sounding	Barnes objectively analyzed radiosonde/wind profilers	Ooyama scale-controlled ship network radiosondes	multiquadratic interpolation of radiosondes
Water vapor mixing ratio sounding	Barnes objectively analyzed radiosonde/wind profilers	Ooyama scale-controlled ship network radiosondes	multiquadratic interpolation of radiosondes
Surface pressure	EBBR	not available	large-scale array [*Lin and Johnson*, 1996a]
		External Parameters	
Solar constant	calculated	calculated	calculated
Latitude, longitude, Julian day, and GMT	calculated	calculated	calculated
Vertical profiles of the horizontal wind components	Barnes objectively analyzed radiosonde/wind profilers	Ooyama scale-controlled ship network radiosondes	multiquadratic interpolation of radiosondes
Surface pressure tendencies	EBBR	not available	large-scale array [*Lin and Johnson*, 1996a]
Large-scale divergence	Barnes objectively analyzed radiosonde/wind profilers	Ooyama scale-controlled ship network radiosondes	multiquadratic interpolation of radiosondes
Tendencies of temperature and water vapor due to horizontal advection	Barnes objectively analyzed radiosonde/wind profilers	Ooyama scale-controlled ship network radiosondes	multiquadratic interpolation of radiosondes
Skin temperature	EBBR	ship measurements	buoy measurements
Surface fluxes of sensible and latent heat	EBBR	not available	buoy measurements
		Data for Model Evaluation	
Precipitation rate	OK/KSU mesonets, SMOS	radar observations	buoy measurements/calculated
All variables for which initial conditions are needed	see above	see above	see above
Surface fluxes of sensible and latent heat	see above	see above	see above

The left column lists the data requirements, and the remaining columns show how these requirements were met for each of the three field programs. EBBR stands for energy balance bowen ratio system, which is used to infer surface fluxes and other quantities at the ARM site [*Oke*, 1978; *Stokes and Schwartz*, 1994]. OK/KSU, Oklahoma/Kansas State University; SMOS, Surface Meteorological Observing System.

clones) dynamically impossible because they cannot be balanced by rotation [*Charney*, 1963]. At the midlatitude ARM site, the temporal fluctuations of temperature and moisture can be much stronger than those observed during GATE and TOGA COARE, and in addition, the horizontal advective tendencies of temperature and moisture can be much more dramatic, especially when frontal passages occur.

4. Model Description

The SCM used here is a single-column version of the Colorado State University GCM. The SCM and the GCM are actually the same computer code; options can be selected at compilation time to control whether the model runs in three-dimensional (GCM) or one-dimensional (SCM) mode. The model uses a stretched vertical coordinate in which the top of the planetary boundary layer (PBL) is a coordinate surface [*Suarez et al*., 1983]. The PBL is then identically the lowest layer of the model. The depth and turbulence kinetic energy of the PBL are prognostic (i.e., time stepped) variables of the model.

The cumulus parameterization is based on the ideas of *Arakawa and Schubert* [1974] but with the prognostic convective closure described by *Randall and Pan* [1993] and *Pan and Randall* [1998] and with multiple cloud-base levels as reported by *Ding and Randall* [1998]. Except as noted, for all runs described in this paper, the parameters α and τ_D, used in the convection parameterization and discussed in detail by *Pan and Randall* [1998], were set to 10^8 m^4 kg^{-1} and 10^3 s, respectively. The model results do depend significantly on the value of α used. The baseline choice, $\alpha = 10^8$ m^4 kg^{-1}, is not necessarily optimal, and in fact, for the example presented in detail in section 5, $\alpha = 10^9$ m^4 kg^{-1} gives noticeably more realistic simulations. This paper is not about cumulus parameterization, and the physical interpretation of α will not be discussed here; such a discussion is given by *Pan and Randall* [1998]. Nevertheless, we will discuss the results of experiments in which the value of α is varied. The purpose of these experiments, in the context of the present paper, is to investigate how the results depend on the method by which the SCM is forced. This allows us to illustrate some important differences among the forcing methods.

The stratiform cloud parameterization used in the model was developed by *Fowler et al*. [1996] and *Fowler and Randall* [1996a, b]. The radiation parameterization is that of *Harshvardhan et al*. [1987]. The model also includes the land-surface parameterization developed by *Sellers et al*. [1996a, b] and tested by *Randall et al*. [1996b], but as already mentioned, the land-surface model is not used in the ARM SCM runs described here; instead, we prescribed the surface fluxes of sensible and latent heat according to observations. For detailed descriptions of the GCM and its performance, see the papers cited above and also *Randall et al*. [1991].

5. Results

5.1. An Example

We begin by presenting in Plate 1, Figure 4, Plate 2, and Figures 5 and 6, the results obtained for one particular case:

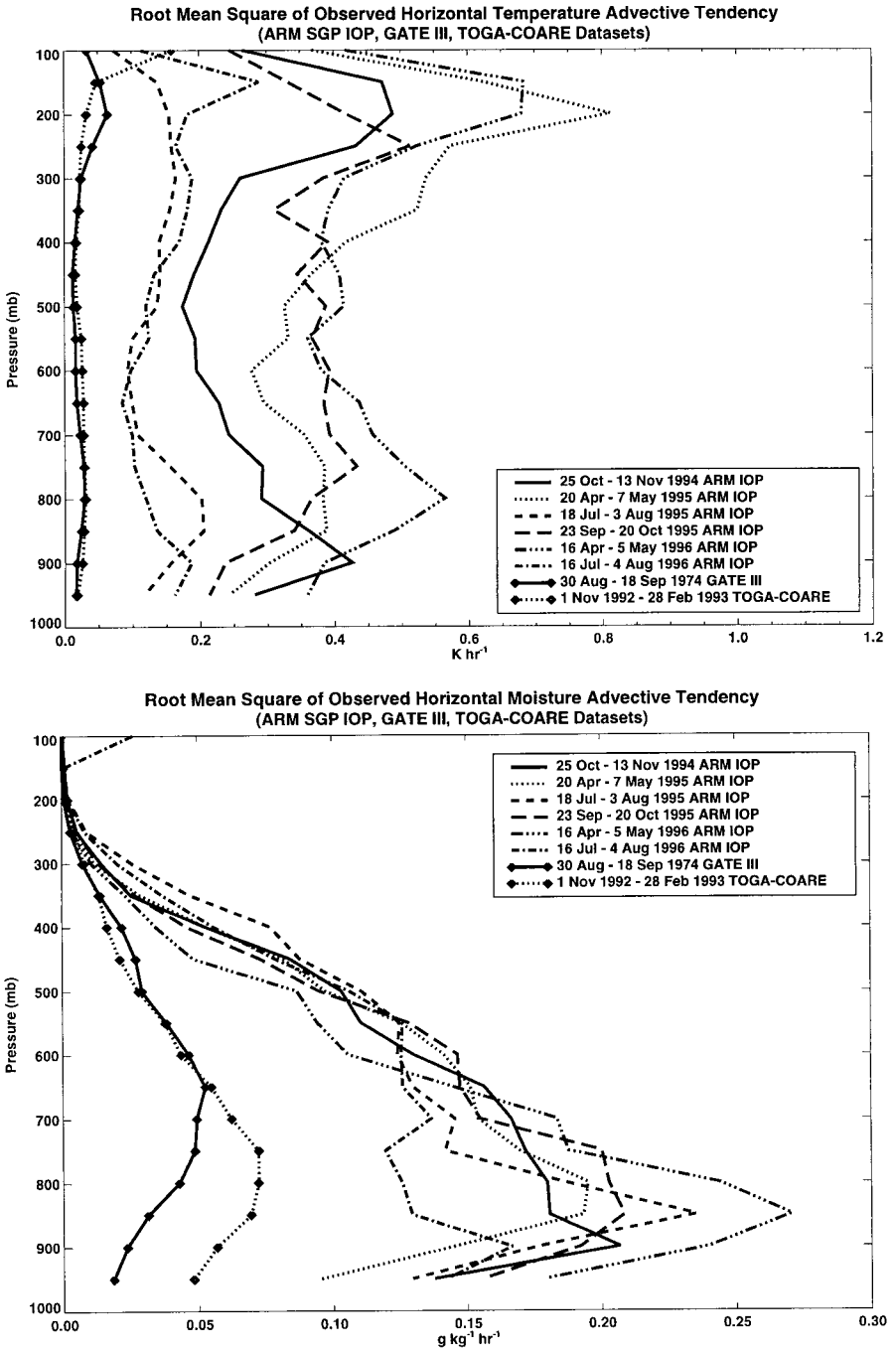

Figure 3. Root-mean-square horizontal advective tendencies of (top) temperature horizontal advective tendency and (bottom) water vapor mixing ratio horizontal advective tendency, as functions of height, for each of the data sets discussed in this paper.

the July 1995 ARM IOP. This case has not been selected to make the model look good; as documented later, the agreement between the simulations and the observations is better for some of the other cases. We have chosen this case as our example because the data are particularly well analyzed and also because this case is the subject of a model intercomparison being conducted by *Ghan et al.* [1999b].

The top four panels of Plate 1 show the time-height evolution of the temperature as observed (top left), as simulated using revealed forcing (RF, top right), as simulated using horizontal advective forcing (HF, middle left), and as simulated using relaxation forcing (XF, middle right). Although all three simulations reproduce some of the gross aspects of the observed temperature changes, such as the low-level warming around day 10, the results obtained with both RF and HF contain large errors and show occasional rapid temporal changes that are not observed. For each of the plots in the top panels of Plate 1 the results from the XF run indicate what a "nearly perfect" model would do, and they are in fact much better than those of the RF and HF runs. The bottom two panels of Plate 1 show the observed (left) and XF-simulated (right) tendencies of temperature due to horizontal advection.

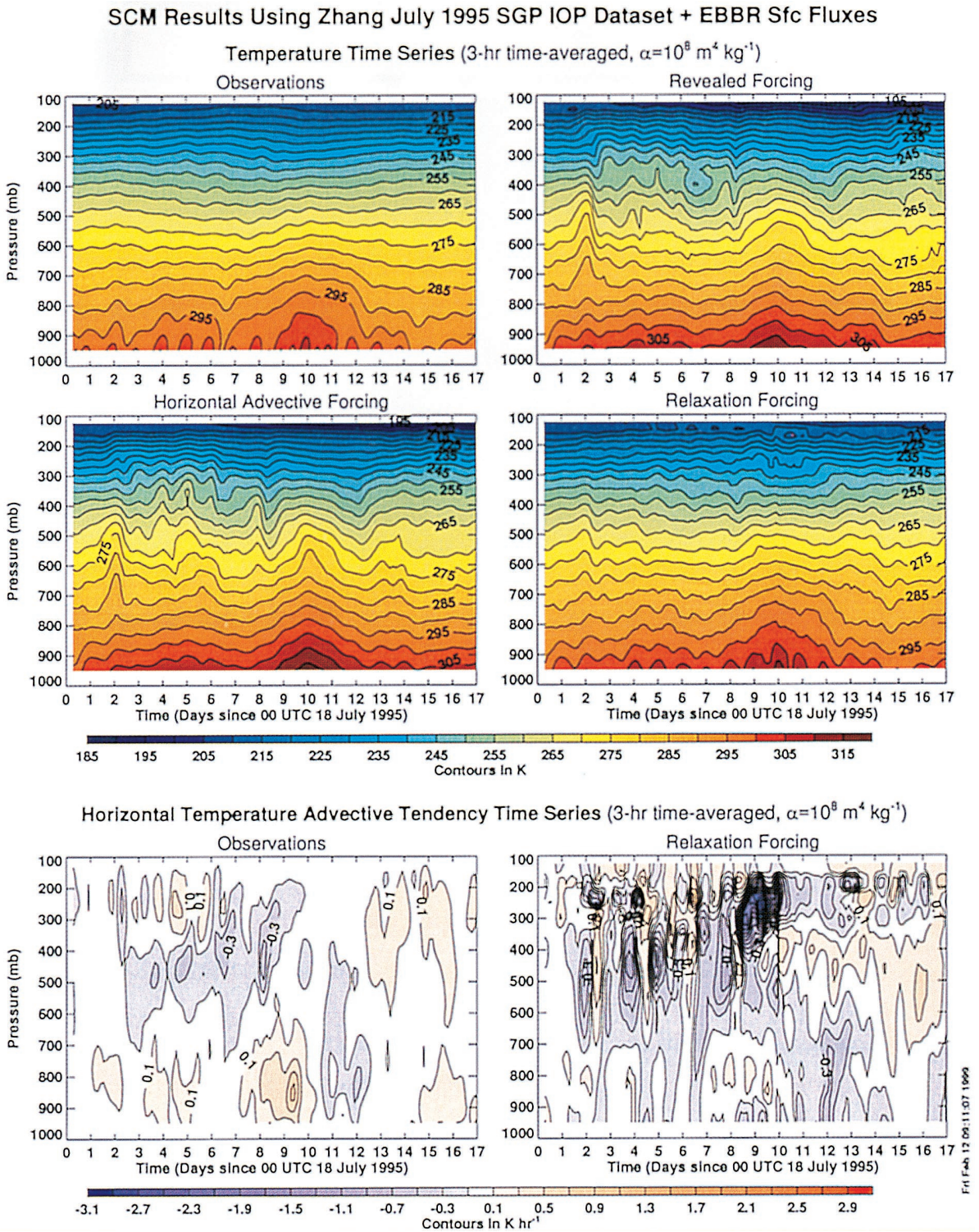

Plate 1. Temperature observations and simulations for the July 1995 ARM IOP: (top left) observations as a function of time and height, (top right) corresponding RF simulation, and (middle left and right) corresponding HF and XF simulations. The bottom panels show the observed (left) and XF-simulated (right) horizontal advective tendencies as functions of time and height.

For this case the agreement is poor. Figure 4 provides additional insight into these results. The mean temperature soundings in all of the runs are fairly realistic, except at the lowest levels where the simulated sounding is too warm. RF and HF overestimate the temporal standard deviation by about a factor of 2, except near the surface. The simulated temporal skewness shows little resemblance to the observations for RH and HF. The temporal correlations between the RF and HF runs and

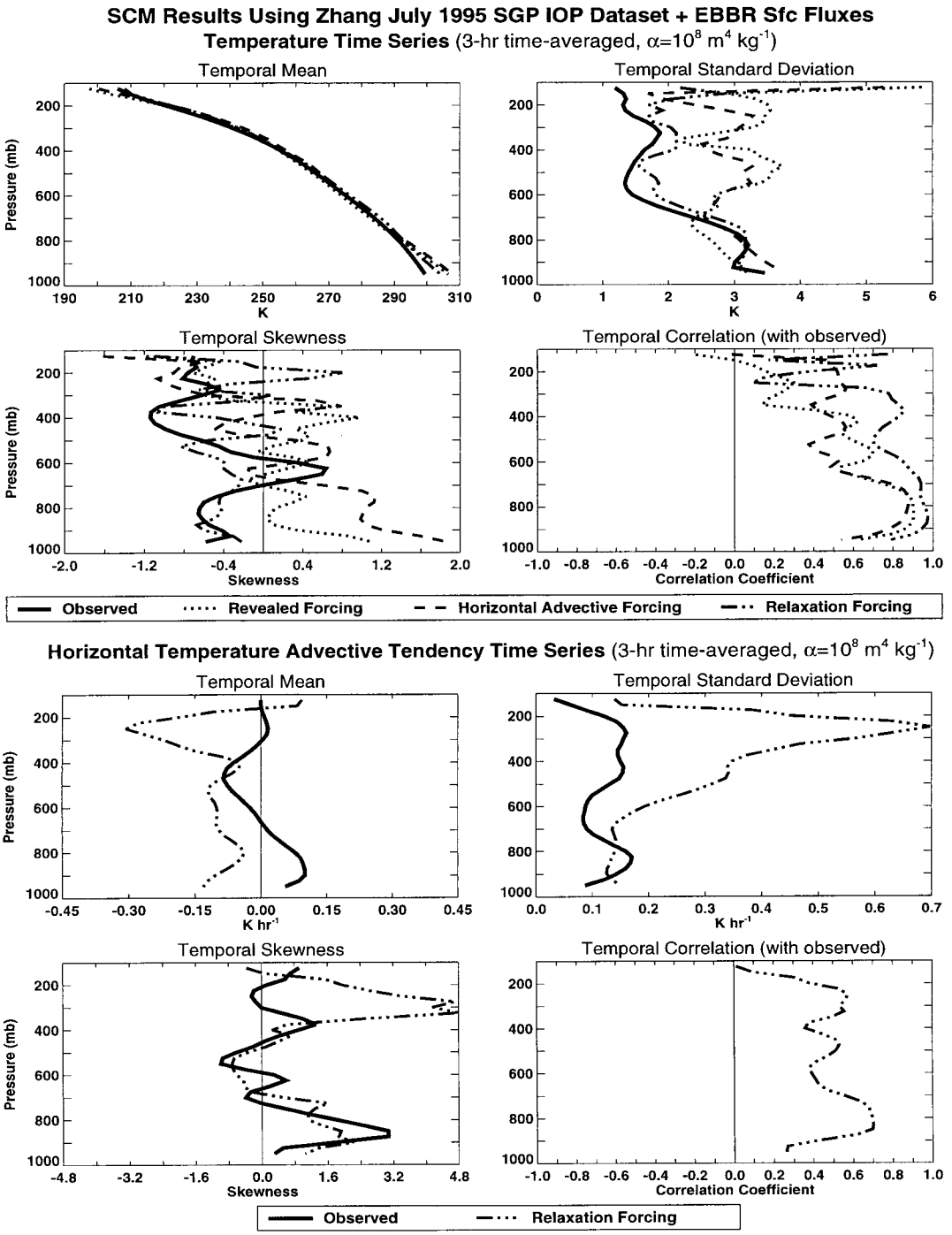

Figure 4. Temperature statistics for the July 1995 ARM IOP: (top left) observed and simulated time-mean temperatures as functions of height, (top right) corresponding temporal standard deviations. The second row shows the temporal skewness (left) and the correlations between each of the simulations and the observations (right). The bottom four panels show similar statistics for the horizontal advective tendency, as observed and as simulated in the XF run.

the observations are fairly good near the surface but drop off significantly in the upper troposphere. The four bottom panels of Figure 4 compare the XF-simulated tendency of temperature due to horizontal advection with the observations. The mean, standard deviation, and skewness are in poor agreement with the observations, but the temporal correlation between the XF results and the observations is moderately encouraging, of the order of 0.5 through most of the troposphere.

Plate 2 and Figure 5 are analogous to Plate 1 and Figure 4, respectively, but for the water vapor field. The RF and HF runs crudely mimic some of the major fluctuations observed but have large errors. Both runs are too dry in the lower troposphere, where the well-mixed PBL becomes excessively deep. As expected, the XF-simulated water vapor profile is considerably more realistic, but the simulated horizontal advective tendency of water vapor is quite different from that observed.

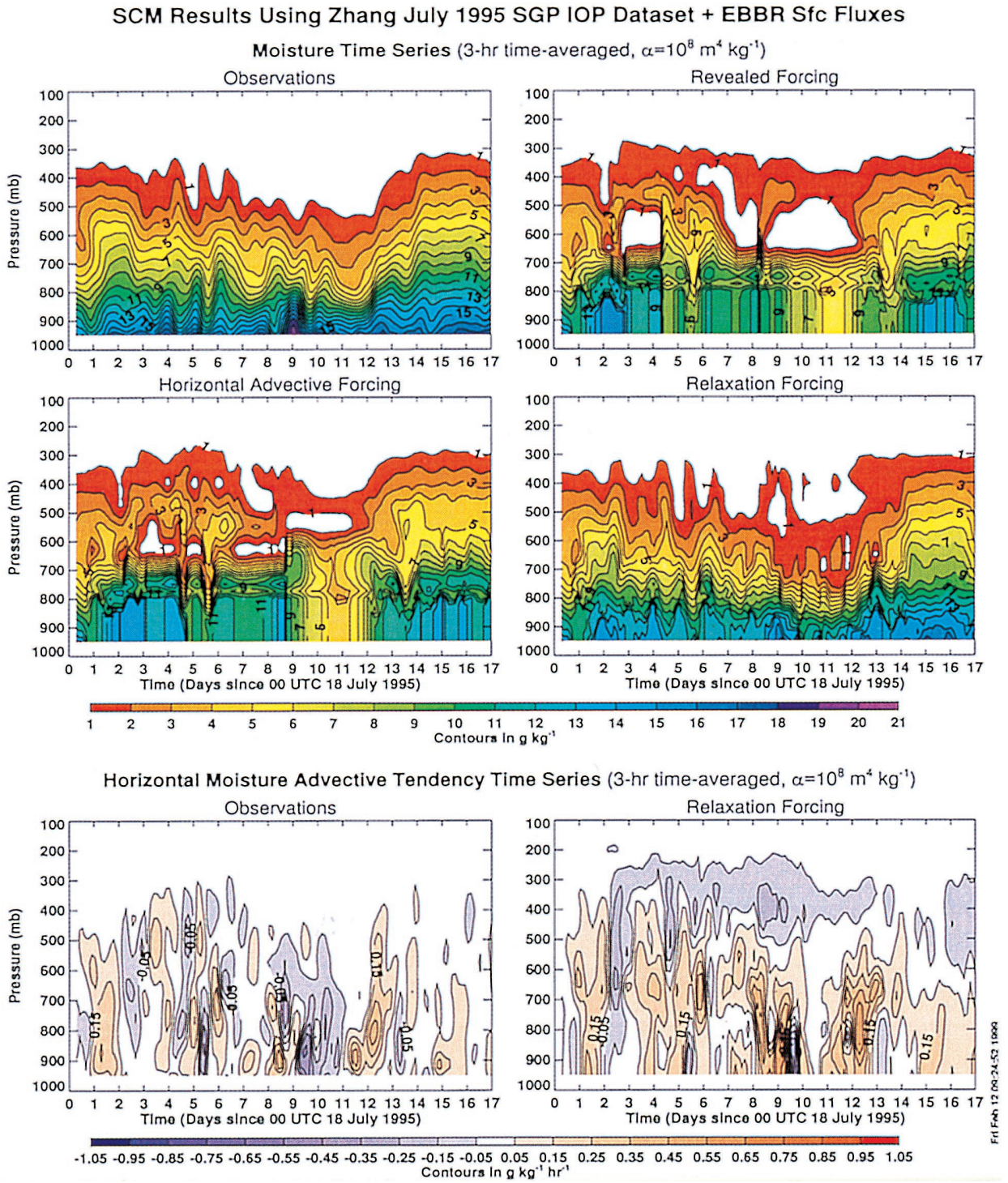

Plate 2. Moisture observations and simulations for the July 1995 ARM IOP: (top left) observations as a function of time and height, (top right) corresponding RF simulation, and (middle left and right) corresponding HF and XF simulations. The bottom panels show the observed (left) and XF-simulated (right) horizontal advective tendencies as functions of time and height.

Figure 5 shows the errors in the mean sounding very clearly. The temporal standard deviations of the RF and HF runs are fairly realistic in the middle troposphere but too large near the surface. The simulated temporal skewness is in fair agreement with the observations. The temporal correlations are also fairly high for the most part. For the XF run, the mean profile of the simulated horizontal advective tendency of water vapor is unrealistic, but the standard deviation is fairly well reproduced, as is the lower-tropospheric skewness, and the temporal correlation between the simulations and the observations is in the range 0.6 to 0.7 at most levels. Overall, the water vapor results are somewhat more realistic than the temperature results.

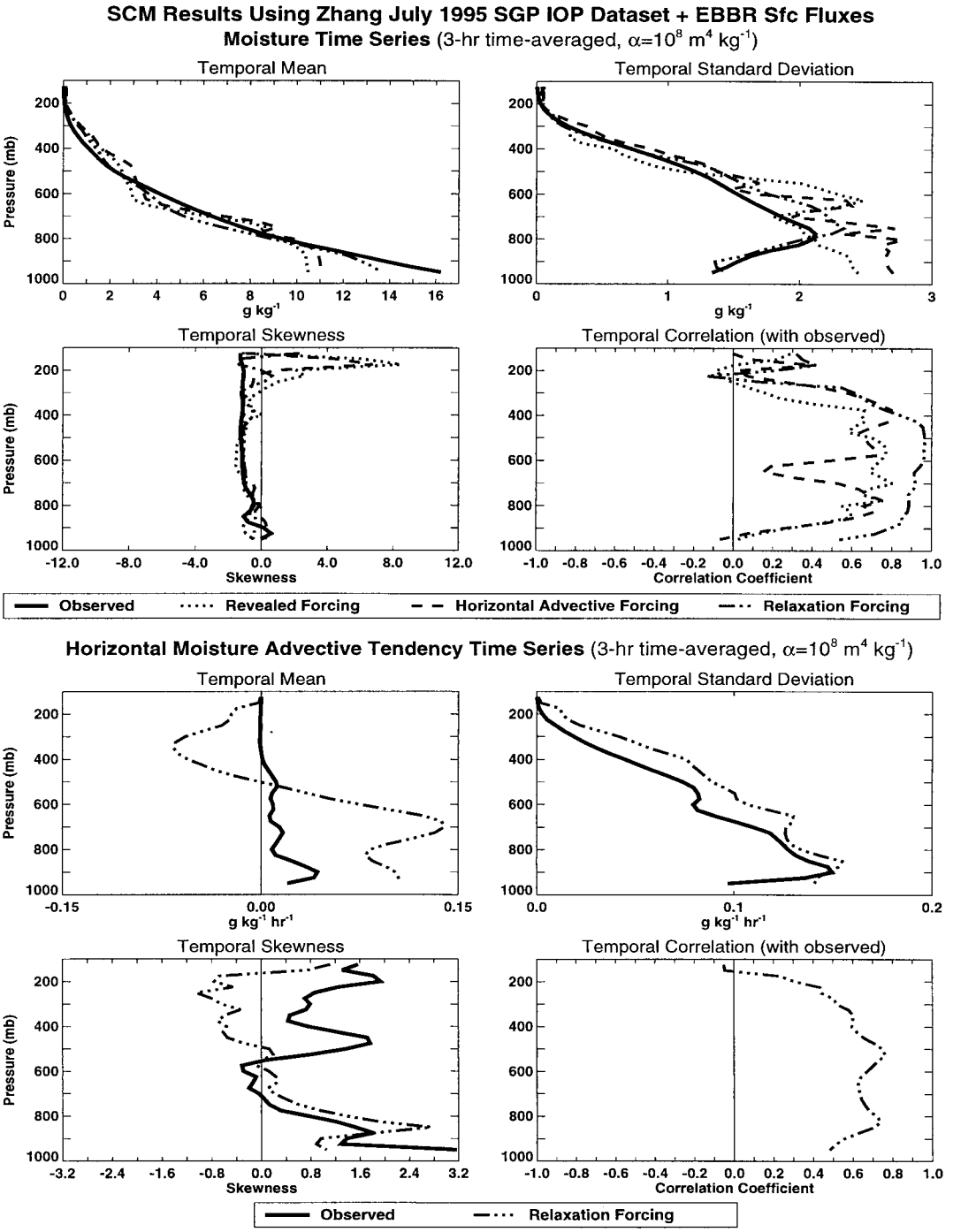

Figure 5. Moisture statistics for the July 1995 ARM IOP: (top left) observed and simulated time-mean temperatures as functions of height, (top right) corresponding temporal standard deviations. The second row shows the temporal skewness (left) and the correlations between each of the simulations and the observations (right). The bottom four panels show similar statistics for the horizontal advective tendency, as observed and as simulated in the XF run.

Figure 6 shows the time series of total column water vapor (PW) and the surface rainfall rate as observed and as simulated in the three runs. The model tends to "run dry"; that is, in each run the simulated atmosphere typically contains less water vapor than observed. The simulated PW results of the three runs are of roughly comparable realism; perhaps surprisingly the mean PW of the XF run is not the most realistic of the three. The precipitation results are interesting, and it is interesting to note that the XF run is by far the least realistic of the three, drastically overestimating the time-average precipitation rate. The results of the RF and HF runs are much more realistic. The reasons for the poor simulated precipitation of the XF run will be explained later.

In summary, this example, based on the July 1995 ARM

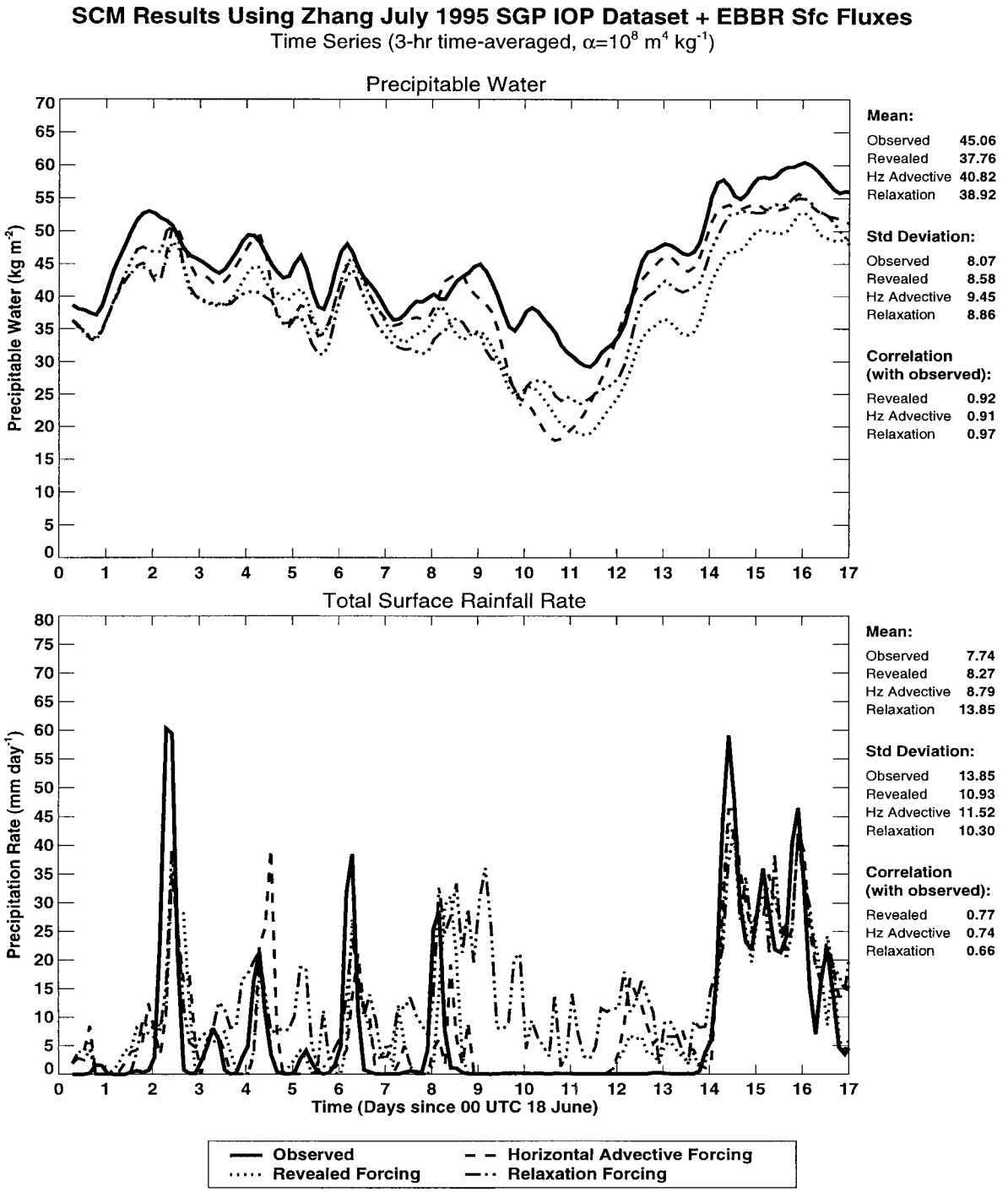

Figure 6. Time series of the simulated and observed total column water vapor (labeled "precipitable water," and shown in the top panel) and surface rainfall rate (bottom) for the July 1995 ARM IOP.

IOP, shows that the RH and HF simulations are only modestly successful in reproducing the observed fluctuations of temperature and water vapor on a level-by-level basis. The observed PW variations are more successfully simulated in these runs, as are the observed surface precipitation variations. Although the temperature and water vapor soundings obtained with relaxation forcing are much more realistic than those obtained with revealed forcing or horizontal advective forcing, the simulated precipitation rate in the XF run is actually much less realistic than in the RF and HF runs. We show below that this holds fairly generally, not just for the particular case discussed here. A simple explanation of this counterintuitive behavior is given later.

5.2. An Overview of All Simulations

In the preceding section we presented our results for the July 1995 ARM IOP. Because of space limitations, we cannot

Table 3. Summary of Results

IOP	α, $m^4\ kg^{-1}$	Forcing	MT	MPW	MPA	MPC	MTA	MTC	MQA	MQC
ARM	10^7	RF	4.801	1.208	1.269	0.489				
Oct. 25 to Nov. 13, 1994		HF	3.932	0.998	0.762	0.409				
		XF	0.485	0.175	0.159	0.409	1.344	0.509	0.888	0.615
	10^8	RF	4.957	1.182	1.247	0.529				
		HF	3.950	0.932	0.745	0.500				
		XF	0.485	0.179	0.118	0.435	1.356	0.507	0.900	0.615
	10^9	RF	5.075	1.182	1.236	0.494				
		HF	3.871	0.871	0.752	0.512				
		XF	0.485	0.180	0.111	0.429	1.358	0.506	0.903	0.615
ARM	10^7	RF	3.588	1.934	0.712	0.466				
April 20 to May 7, 1995		HF	2.745	1.690	0.689	0.416				
		XF	0.517	0.396	0.636	0.572	1.236	0.623	1.321	0.429
	10^8	RF	3.348	2.071	0.680	0.478				
		HF	2.657	1.972	0.744	0.444				
		XF	0.493	0.341	0.217	0.579	1.212	0.645	1.164	0.500
	10^9	RF	3.106	2.164	0.602	0.498				
		HF	2.477	2.100	0.714	0.449				
		XF	0.490	0.336	0.114	0.431	1.224	0.645	1.155	0.525
ARM	10^7	RF	2.212	1.609	1.116	0.727				
July 18 to Aug. 3, 1995		HF	2.598	1.255	1.068	0.706				
		XF	1.476	1.294	2.932	0.593	3.240	0.345	2.048	0.382
	10^8	RF	1.720	0.999	1.069	0.762				
		HF	1.790	0.714	1.135	0.736				
		XF	1.094	0.812	1.789	0.654	2.352	0.466	1.298	0.448
	10^9	RF	1.767	0.566	1.072	0.794				
		HF	1.698	0.785	1.127	0.785				
		XF	0.790	0.503	0.720	0.744	1.809	0.503	0.885	0.519
ARM	10^7	RF	2.851	0.986	1.418	0.413				
Sept. 23 to Oct. 20, 1995		HF	3.149	1.045	1.702	0.323				
		XF	0.466	0.200	1.375	−0.001	1.040	0.619	0.876	0.496
	10^8	RF	2.904	1.030	1.427	0.251				
		HF	3.297	1.162	1.867	0.362				
		XF	0.445	0.173	0.385	0.008	0.990	0.665	0.812	0.527
	10^9	RF	3.287	1.010	1.281	0.329				
		HF	3.596	1.262	1.922	0.354				
		XF	0.439	0.173	0.053	0.007	0.989	0.673	0.800	0.556
ARM	10^7	RF	3.139	1.153	1.612	0.560				
April 16 to May 5, 1996		HF	2.672	1.349	0.954	0.831				
		XF	0.401	0.296	2.501	0.299	1.068	0.642	1.078	0.399
	10^8	RF	3.322	1.103	1.412	0.525				
		HF	2.534	1.255	1.024	0.750				
		XF	0.367	0.238	0.731	0.243	1.013	0.678	0.874	0.497
	10^9	RF	3.364	1.094	1.327	0.488				
		HF	2.277	1.187	1.121	0.697				
		XF	0.357	0.255	0.093	0.270	1.017	0.684	0.871	0.530
ARM	10^7	RF	3.262	3.390	0.860	0.531				
July 16 to Aug. 4, 1996		HF	3.089	2.774	0.528	0.491				
		XF	0.982	0.675	2.013	0.111	2.161	0.362	1.320	0.466
	10^8	RF	3.332	3.132	0.829	0.669				
		HF	3.090	2.385	0.483	0.521				
		XF	0.781	0.448	0.942	0.103	1.822	0.452	1.003	0.515
	10^9	RF	4.000	3.010	0.790	0.631				
		HF	3.380	2.084	0.430	0.649				
		XF	0.650	0.427	0.194	0.223	1.901	0.486	0.883	0.574
GATE	10^7	RF	3.262	3.390	0.860	0.531				
		HF	3.089	2.774	0.528	0.491				
		XF	0.982	0.675	2.013	0.111	2.161	0.362	1.320	0.466
	10^8	RF	3.332	3.132	0.829	0.669				
		HF	3.090	2.385	0.483	0.521				
		XF	0.781	0.448	0.942	0.103	1.822	0.452	1.003	0.515
	10^9	RF	4.000	3.010	0.790	0.631				
		HF	3.380	2.084	0.430	0.649				
		XF	0.650	0.427	0.194	0.223	1.901	0.486	0.883	0.574
TOGA COARE	10^7	RF	1.412	5.249	0.876	0.750				
		HF	1.415	5.652	0.633	0.589				
		XF	1.379	1.697	1.578	0.544	4.622	0.032	1.878	0.040
	10^8	RF	1.407	4.898	0.867	0.791				
		HF	1.395	4.601	0.683	0.735				
		XF	1.367	1.245	1.242	0.557	4.070	0.018	1.554	0.040
	10^9	RF	1.411	4.905	0.858	0.782				
		HF	1.393	3.362	0.760	0.758				
		XF	1.359	1.053	0.778	0.654	3.939	−0.007	1.504	0.041

give comparable discussions of each of the many additional simulations performed in the course of this study; instead, we provide, in Table 3, a summary of the results obtained. For each run, the table gives values of the following nondimensional figures of merit: (1) MT, the vertical integral of the root-mean-square (rms) temperature error, normalized by the vertically integrated temporal standard deviation of the temperature; (2) MPW, the temporal rms PW error, normalized by the temporal standard deviation of the PW; (3) MPA, the ratio of the simulated and observed time-averaged surface precipitation rates; and (4) MPC, the temporal correlation of the simulated and observed surface precipitation rates. Obviously for a "perfect simulation" (i.e., a simulation obtained using a perfect model with perfect input data) the first two figures of merit would be equal to zero, and the second two figures would be equal to 1. Only the fourth can be negative, even in principle, and of course, we hope that negative values will not be encountered in practice.

In addition, and only for the runs with relaxation forcing, we tabulate the following: (1) MTA, the vertical integral of the temporal rms error in the tendency of temperature due to horizontal advection, normalized by the vertical integral of the rms value of the observed tendency of temperature due to horizontal advection; (2) MTC, the vertical average of the temporal correlation of the observed and simulated tendencies of temperature due to horizontal advection; (3) MQA, the vertical integral of the rms error in the tendency of water vapor due to horizontal advection, normalized by the vertical integral of the rms value of the observed tendency of water vapor due to horizontal advection; and (4) MQC, the vertical average of the temporal correlation of the observed and simulated tendencies of water vapor due to horizontal advection. In a perfect simulation, MTA and MQA would be equal to zero, while MTC and MQC would be equal to 1.

There are eight observed cases (six ARM IOPs, GATE, and TOGA COARE). For each case we have three runs; and each run has been performed for three different values of α. Altogether, then, Table 3 summarizes the results from 72 SCM integrations. The sheer size of the table illustrates one of the strengths of single-column modeling: many simulations can be performed and analyzed with relative speed and ease.

Overall, the results presented here do not show unambiguous differences between revealed forcing and horizontal advective forcing. The two methods appear to be generally comparable. Revealed forcing may therefore be preferred for its simplicity. This conclusion is of course tentative and subject to revision in light of further analyses.

Figure 7 shows the root-mean-square errors for the vertically integrated temperature, the total column water vapor, and the precipitation rate for each of the various cases considered and for three different values of α. Here the "error" in each case is the difference between the simulation and the observation, and "mean" refers to the time average over the entire simulation. The vertical axes show the errors for revealed forcing, and the horizontal axes show the errors for horizontal advective forcing. Along the diagonal line, the two root-mean-square errors are equal. For the vertically integrated temperature and total column water vapor, revealed forcing gives larger errors overall. For the precipitation rate, horizontal advective forcing gives larger errors overall, with the exception of one of the ARM IOPs.

As shown in Figure 8, the XF runs can reproduce the observed horizontal advective tendencies most successfully when those tendencies are large. Here results are shown for $\alpha = 10^8$ $m^4\,kg^{-1}$ only. The observed advective tendency of temperature is very poorly simulated for GATE and TOGA COARE, simply because the observed tendencies are tiny in those cases. A small error in the simulation can easily mask the small observed tendency, preventing it from being accurately diagnosed. In addition, the small observed values probably contain large fractional uncertainties.

An implication of this result is that relaxation forcing is not suitable for use in the tropics because the observed tropical horizontal advective tendencies are so small that they cannot be accurately diagnosed, thus limiting our ability to compare model results with observations.

Relaxation forcing gives the most realistic soundings. Nevertheless, in many cases, relaxation forcing gives the least realistic surface precipitation rate. The reasons for this are explored in section 5.3.

5.3. Variations With α

Inspection of Table 3 shows that in general, the model tends to produce more humid (in the sense of total column water vapor) soundings when α is large and drier soundings when α is small. The top panel of Figure 9 shows graphically that in particular, this is true for the XF runs. When convection is active the simulated atmosphere becomes drier as α decreases. For $\alpha = 10^7$ $m^4\,kg^{-1}$, the simulated atmosphere is considerably drier than observed, while for $\alpha = 10^9$ $m^4\,kg^{-1}$, it is slightly more humid than observed. In short, for small α the model "runs dry," while for large α, it "runs wet." The physical explanation for this is discussed by *Pan and Randall* [1998]; for purposes of the present paper, this explanation is irrelevant. Here we simply take advantage of the fact that we can make the model run wet or run dry by altering the value of α.

As already discussed, the precipitation rate tends to be very unrealistic in the XF runs, despite the fact that the XF-simulated soundings are generally more realistic in the XF runs. Figure 9 and Table 3 show that for the XF runs with small α the precipitation rate is higher, while with larger α, it is lower. This is particularly true for those IOPs in which con-

Table 3. (continued) RF, revealed forcing; HF, horizontal advective forcing; XF, relaxation forcing. MT, the vertical integral of the root-mean-square (rms) temperature error, normalized by the observed vertically integrated temporal standard deviation of the temperature; MPW, the temporal rms PW error, normalized by the observed temporal standard deviation of the PW; MPA, the ratio of the simulated and observed time-averaged surface precipitation rates; MPC, the temporal correlation of the simulated and observed surface precipitation rates; MTA, the vertical integral of the temporal rms error in the tendency of temperature due to horizontal advection, normalized by the vertical integral of the rms value of the observed tendency of temperature due to horizontal advection; MTC, the vertical average of the temporal correlation of the observed and simulated tendencies of temperature due to horizontal advection; MQA, the vertical integral of the rms error in the tendency of water vapor due to horizontal advection, normalized by the vertical integral of the rms value of the observed tendency of water vapor due to horizontal advection; MQC, the vertical average of the temporal correlation of the observed and simulated tendencies of water vapor due to horizontal advection.

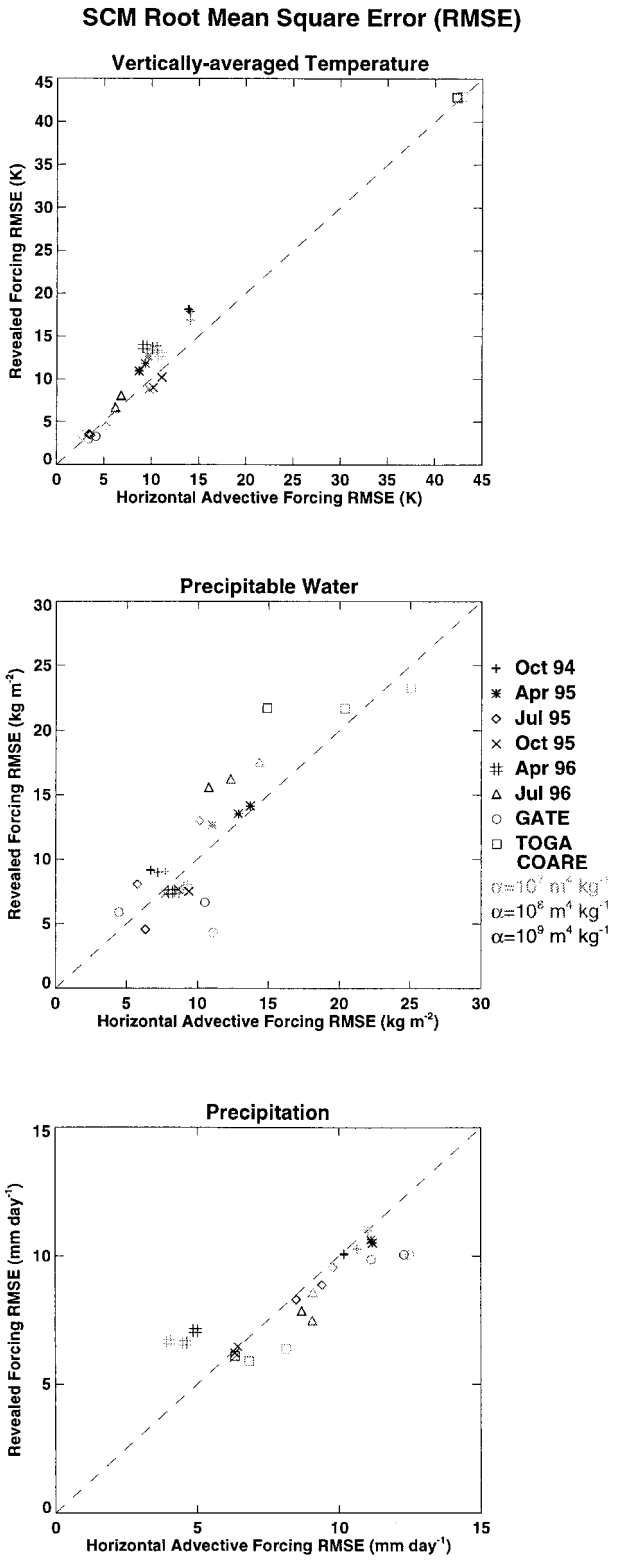

Figure 7. Root-mean-square errors for the vertically integrated temperature (top), the total column water vapor (middle), and the precipitation rate (bottom) for the various cases considered and for three different values of α. Here the "error" in each case is the difference between the simulation and the observation, and "mean" refers to the time average over the entire simulation. The vertical axes show the errors for revealed forcing, and the horizontal axes show the errors for horizontal advective forcing. Along the diagonal line, the two root-mean-square errors are equal.

vection was active. Table 4 provides indices of the degree to which the IOP weather was influenced by convection. These indices are based on the amount of convective precipitation and total precipitation produced in RF simulations, with $\alpha = 10^8$ m^4 kg^{-1}.

The interpretation of these results is very simple: In a model that tends to run drier than observed (i.e., with small α), relaxation forcing fights back against this drying by trying to moisten the sounding, and the parameterizations of the model, in turn, fight back against the relaxation by drying the sounding through precipitation. As a result, relaxation forcing leads to excessive precipitation in a model that tends to run dry. In a model that tends to run wet, relaxation forcing tends to dry out the sounding, and so inhibits precipitation.

These results indicate that "error is conserved." With RF and HF forcing, the precipitation rates are relatively realistic but the soundings deviate substantially from the observations, and this tells us that something is wrong with the model. With XF forcing, the soundings are guaranteed to be relatively realistic, but the precipitation rates deviate greatly from the observations, telling us again that there are problems with the model. This indicates that relaxation does not hide the problems of a model; it only changes the way in which those problems manifest themselves.

6. Summary and Conclusions

We have explored several approaches to prescribing observed forcing for use in SCMs and CSMs, and we have presented results obtained with the various methods for several different observed cases. Not surprisingly, each approach has certain advantages and disadvantages.

At the end of section 2 we offered some hypotheses as to which forcing methods would give the most realistic model results. Note, however, that it is not (or should not be) our goal to choose the forcing method which gives the most realistic results. The scientific payoff comes when model deficiencies are identified, because this presents us with an opportunity to learn something new. Therefore our goal should be to subject the model to the forcing method or methods which most readily expose its weaknesses.

The results presented in this paper show that relaxation forcing can very clearly reveal certain types of model deficiencies which might be overlooked in studies based on revealed and/or horizontal advective forcing. Our results suggest that revealed forcing gives larger errors in the soundings, while

Table 4. Measures of the Degree to Which Cumulus Convection Influenced the Weather in Each of Eight IOPs

IOP	Convective Precipitation, mm d^{-1}	Convective Precipitation As a Fraction of All Precipitation
ARM		
Oct. 25 to Nov. 13, 1994	0.577	0.172
April 20 to May 7, 1995	1.850	0.341
July 18 to Aug. 3, 1995	5.468	0.706
Sept. 23 to Oct. 20, 1995	0.727	0.532
April 16 to May 5, 1996	0.404	0.248
July 16 to Aug. 4, 1996	2.367	0.519
GATE	10.259	0.899
TOGA COARE	4.180	0.449

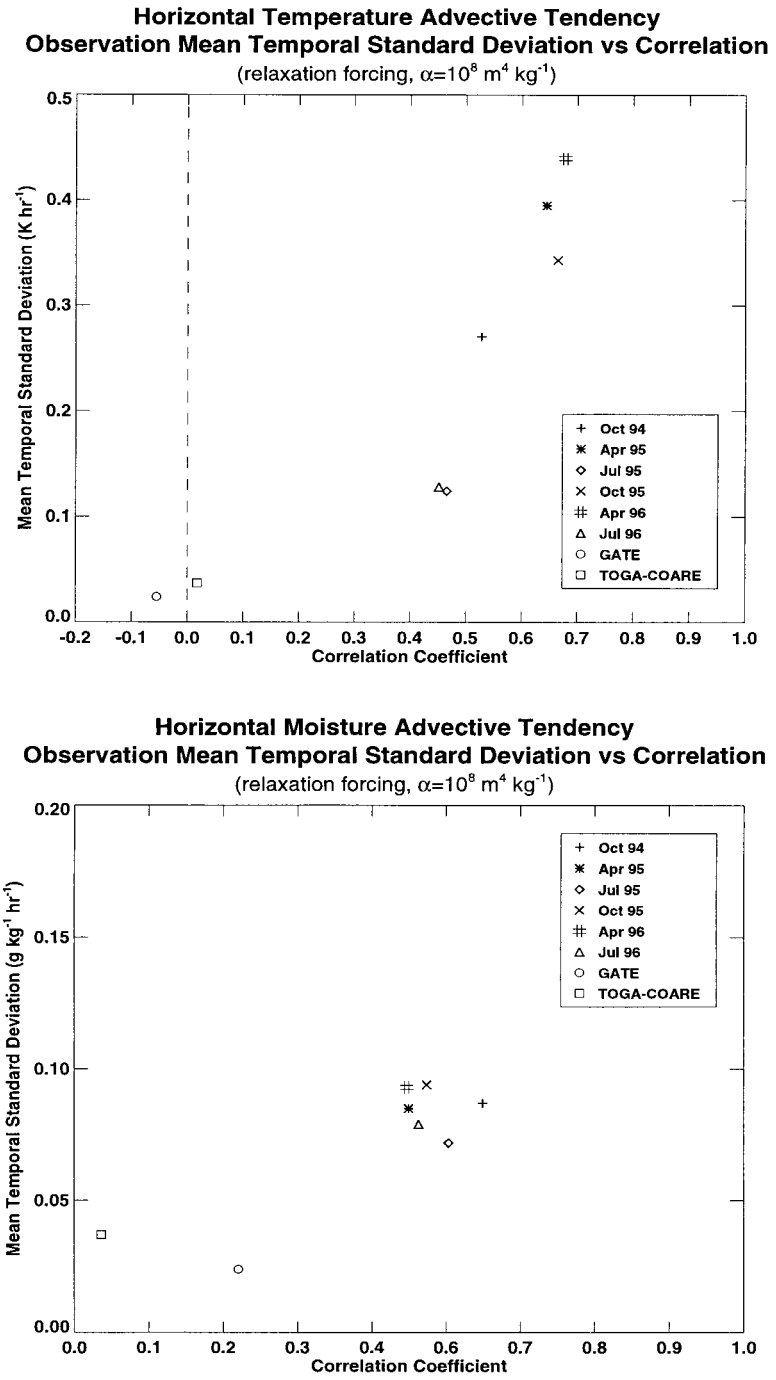

Figure 8. For the various XF simulations the horizontal axis represents the correlation of the diagnosed horizontal advective tendency with the corresponding observations, and the vertical axis represents the standard deviation of the observed horizontal advective tendency. Here we show only results obtained with $\alpha = 10^8$ m^4 kg^{-1}. When the observed standard deviation is high, the correlation is high.

horizontal advective forcing gives larger errors in the precipitation rate. The differences are fairly small and may not be significant. Further study is needed on this point. Our results clearly demonstrate that relaxation forcing is not well suited for use with tropical data sets, because the observed tendencies of temperature and water vapor are so small in the tropics that it is virtually impossible to diagnose them accurately in terms of model output, using the methods discussed in this paper.

Acknowledgments. This study has been supported by the U.S. Department of Energy ARM Program under grant DE-FG02-92ER61363 to Colorado State University. TOGA COARE data were kindly provided by Richard Johnson and Paul Ciesielski of Colorado State University. Ric Cederwall, Jon Yio, and Marty Leach of the Lawrence Livermore National Laboratory were instrumental in providing the ARM data used in this study. It has been a pleasure working with them. Steve Ghan of the Pacific Northwest Laboratories made helpful comments on a preliminary draft of the manuscript.

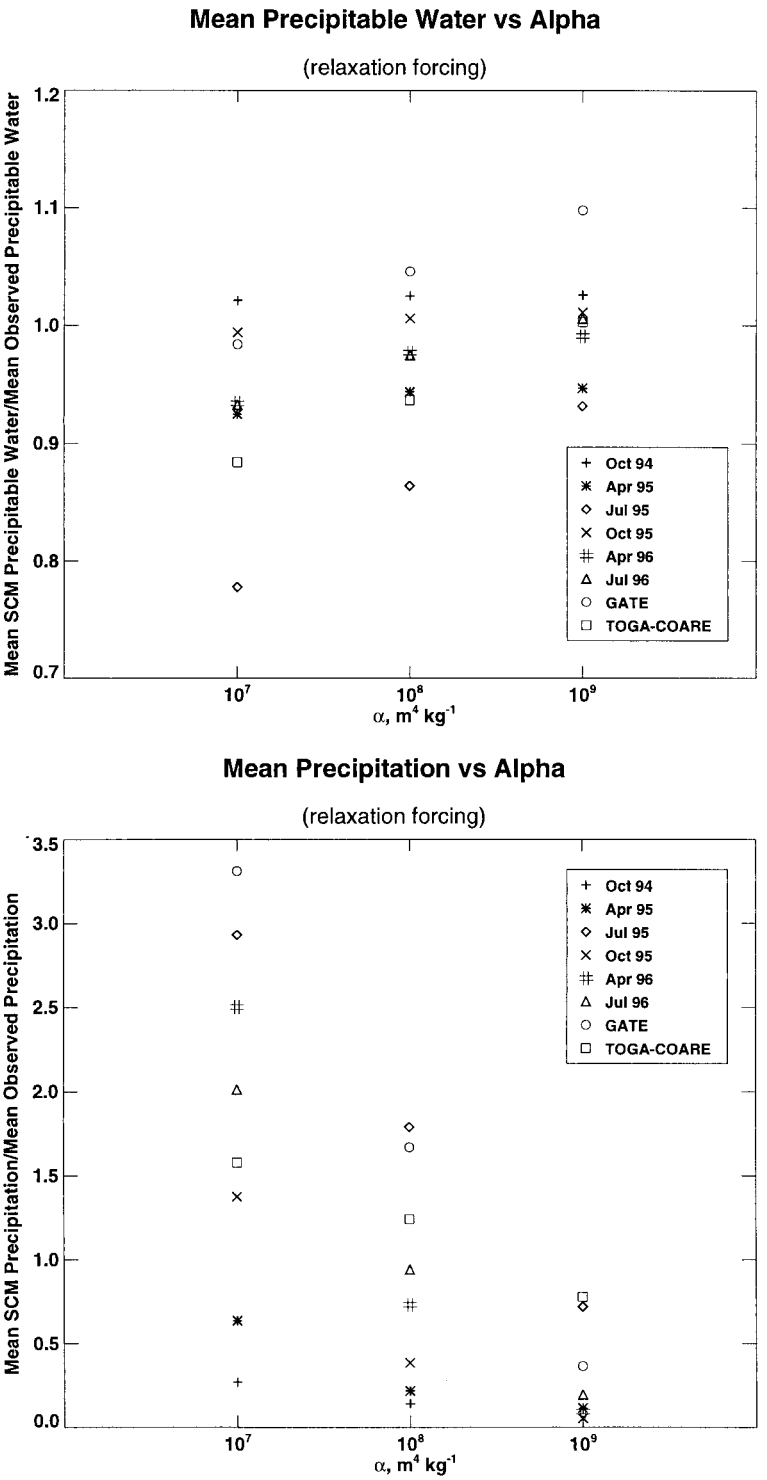

Figure 9. Plots of the mean total column water vapor (top) and mean precipitation rate (bottom) as functions of α, for the various cases, with relaxation forcing.

References

Arakawa, A., and W. H. Schubert, The interaction of a cumulus cloud ensemble with the large-scale environment, I, *J. Atmos. Sci.*, *31*, 674–701, 1974.

Barnes, S. L., A technique for maximizing details in numerical weather map analysis, *J. Appl. Meteorol.*, *3*, 396–409, 1964.

Bechtold, P., et al., A GCSS model intercomparison for a tropical squall line observed during TOGA-COARE, II, Intercomparison of SCMs with CRM, *Q. J. R. Meteorol. Soc.*, in press, 1998.

Betts, A. K., and M. J. Miller, A new convective adjustment scheme, II, Single column tests using GATE wave, BOMEX, ATEX, and arctic air-mass data sets, *Q. J. R. Meteorol. Soc.*, *112*, 693–709, 1986.

Browning, K. A., The GEWEX Cloud System Study (GCSS), *Bull. Am. Meteorol. Soc.*, *74*, 387–399, 1993.

Charney, J. G., A note on large-scale motions in the tropics, *J. Atmos. Sci.*, *20*, 607–609, 1963.

Ding, P., and D. A. Randall, A cumulus parameterization with multiple cloud-base levels, *J. Geophys. Res.*, *103*, 11,341–11,354, 1998.

Fowler, L. D., and D. A. Randall, Liquid and ice cloud microphysics in

the CSU general circulation model, 2, Simulation of the Earth's radiation budget, *J. Clim*., *9*, 530–560, 1996a.

Fowler, L. D., and D. A. Randall, Liquid and ice cloud microphysics in the CSU general circulation model, 3, Sensitivity tests, *J. Clim*., *9*, 561–586, 1996b.

Fowler, L. D., D. A. Randall, and S. A. Rutledge, Liquid and Ice Cloud Microphysics in the CSU General Circulation Model, 1, Model description and simulated microphysical processes, *J. Clim*., *9*, 489–529, 1996.

Ghan, S. J., L. R. Leung, and J. McCaa, A comparison of three different modeling strategies for evaluating cloud and radiation parameterizations, *Mon. Weather Rev*., in press, 1999a.

Ghan, S. J., et al., An intercomparison of single-column model simulations of summertime midlatitude continental convection, *J. Geophys. Res*., in press, 1999b.

Harshvardhan, R. Davies, D. A. Randall, and T. G. Corsetti, A fast radiation parameterization for atmospheric circulation models, *J. Geophys. Res*., *92*, 1009–1016, 1987.

Hudlow, M. D., and V. L. Patterson, GATE radar rainfall atlas, *NOAA Spec. Rep*., 155 pp., 1979.

Krueger, S. K., Numerical simulation of tropical cumulus clouds and their interaction with the subcloud layer, *J. Atmos. Sci*., *45*, 2221–2250, 1988.

Leach, M. J., J. Yio, and R. T. Cederwall, Estimation of errors in objectively analyzed fields and sensitivity to number and spacing of stations, in *Proceedings of the Sixth Annual Atmospheric Radiation Measurement* (*ARM*) *Science Team Meeting*, *DOE CONF-9603149*, pp. 149–151, Dep. of Energy, Washington, D. C., 1996. (Available from the U.S. Dep. of Comm., Technol. Admin., Natl. Tech. Inf. Serv., Springfield, Va.)

Leach, M. J., J. Yio, and R. T. Cederwall, Improvements in the LLNL objective analysis scheme for deriving forcing fields for single-column models using ARM data, in *Proceedings of the Seventh Annual Atmospheric Radiation Measurement* (*ARM*) *Science Team Meeting*, *DOE CONF-970365*, pp. 263–266, Dep. of Energy, Washington, D. C., 1997. (Available from the U.S. Dep. of Comm., Technol. Admin., Natl. Tech. Inf. Serv., Springfield, Va.)

Lin, X., and R. H. Johnson, Kinematic and thermodynamic characteristics of the flow over the western Pacific warm pool during TOGA COARE, *J. Atmos. Sci*., *53*, 695–715, 1996a.

Lin, X., and R. H. Johnson, Heating, moistening, and rainfall over the western Pacific warm pool during TOGA COARE, *J. Atmos. Sci*., *53*, 3367–3383, 1996b.

Nuss, W. A., D. W. Titley, and W. David, Use of multiquadratic interpolation for meteorological objective analysis, *Mon. Weather Rev*., *122*, 1611–1631, 1994.

O'Brien, J. J., Alternative solutions to the classical vertical velocity problem, *J. Appl. Meteorol*., *9*, 197–203, 1970.

Oke, T. R., *Boundary Layer Climates*, 372 pp., Methuen, New York, 1978.

Ooyama, K., Scale-controlled objective analysis, *Mon. Weather Rev*., *115*, 2476–2506, 1987.

Pan, D.-M., and D. A. Randall, A cumulus parameterization with a prognostic closure, *Q. J. R. Meteorol. Soc*., *124*, 949–981, 1998.

Randall, D. A., and D.-M. Pan, Implementation of the Arakawa-Schubert cumulus parameterization with a prognostic closure, in *Cumulus Parameterization*, *Meteorol. Monogr*., edited by K. Emanuel and D. Raymond, pp. 137–144, Am. Meteorol. Soc., Boston, Mass., 1993.

Randall, D. A., Harshvardhan, and D. A. Dazlich, Diurnal variability of the hydrologic cycle in a general circulation models, *J. Atmos. Sci*., *48*, 40–62, 1991.

Randall, D. A., K.-M. Xu, R. J. C. Somerville, and S. Iacobellis, Single-column models and cloud ensemble models as links between observations and climate models, *J. Clim*., *9*, 1683–1697, 1996a.

Randall, D. A., et al., A Revised Land-Surface Parameterization (SiB2) for Atmospheric GCMs, 3, The greening of the CSU general circulation model, *J. Clim*., *9*, 738–763, 1996b.

Redelsperger, J. L., et al., A GCSS model intercomparison for a tropical squall line observed during TOGA-COARE, I, Cloud resolving models, *Q. J. R. Meteorol. Soc*., in press, 1998.

Reed, R. J., D. C. Norquist, and E. Recker, The structure and properties of African wave disturbances as observed during Phase III of GATE, *Mon. Weather Rev*., *105*, 317–333, 1977.

Sellers, P. J., D. A. Randall, G. J. Collatz, J. Berry, C. Field, D. A. Dazlich, C. Zhang, and L. Bounoua, A revised land-surface parameterization (SiB2) for atmospheric GCMs, 1, Model formulation, *J. Clim*., *9*, 676–705, 1996a.

Sellers, P. J., S. O. Los, C. J. Tucker, C. O. Justice, D. A. Dazlich, G. J. Collatz, and D. A. Randall, A revised land-surface parameterization (SiB2) for atmospheric GCMs, 2, The generation of global fields of terrestrial biophysical parameters from satellite data, *J. Clim*., *9*, 706–737, 1996b.

Stokes, G. M., and S. E. Schwartz, The Atmospheric Radiation Measurement (ARM) Program: Programmatic background and design of the cloud and radiation test bed, *Bull. Am. Meteorol. Soc*., *75*, 1201–1221, 1994.

Suarez, M., A. Arakawa, and D. A. Randall, Parameterization of the planetary boundary layer in the UCLA general circulation model: Formulation and results, *Mon. Weather Rev*., *111*, 2224–2243, 1983.

Thompson, R. M., S. W. Payne, E. Recker, and R. J. Reed, Structure and properties of synoptic scale wave disturbances in the Intertropical Convergence Zone of the eastern Atlantic, *J. Atmos. Sci*., *36*, 53–72, 1979.

Yanai, M., S. K. Esbensen, and J.-H. Chu, Determination of bulk properties of tropical cloud clusters from large-scale heat and moisture budgets, *J. Atmos. Sci*., *30*, 611–627, 1973.

Zhang, C., D. A. Randall, and C.-H. Moeng, M. Branson, K. A. Moyer, and Q. Wang, A surface flux parameterization based on the vertically averaged turbulence kinetic energy, *Mon. Weather Rev*., *124*, 2521–2536, 1996.

Zhang, M. H., and J. L. Lin, Constrained variational analysis of sounding data based on column-integrated budgets of mass, moisture and momentum: Approach and application to ARM measurements, *J. Atmos. Sci*., *54*, 1503–1524, 1997.

D. G. Cripe and D. A. Randall, Dep. of Atmospheric Science, Colorado State University, Fort Collins, CO 80523. (randall@atmos.colostate.edu)

(Received March 11, 1999; revised July 2, 1999;
accepted July 8, 1999.)